nature climate change

ARTICLES

https://doi.org/10.1038/s41558-020-0757-5

Coldest Canadian Arctic communities face greatest reductions in shorefast sea ice

Sarah W. Cooley[1,2]✉, Jonathan C. Ryan[2], Laurence C. Smith[1,2], Chris Horvat[1,2], Brodie Pearson[1,3], Brigt Dale[4] and Amanda H. Lynch[1,2]

Shorefast sea ice comprises only about 12% of global sea-ice cover, yet it has outsized importance for Arctic societies and ecosystems. Relatively little is known, however, about the dominant drivers of its breakup or how it will respond to climate warming. Here, we use 19 years of near-daily satellite imagery to document the timing of shorefast ice breakup in 28 communities in northern Canada and western Greenland that rely on shorefast ice for transportation and traditional subsistence activities. Breakup timing is strongly correlated with springtime air temperature, but the sensitivity of the relationship varies substantially among communities. We combine these observations with future warming scenarios to estimate an annual reduction of 5–44 days in the length of the springtime shorefast ice season by 2100. Paradoxically, the coldest communities are projected to experience the largest reductions in springtime ice season duration. Our results emphasize the local nature of climate change and its varied impacts on Arctic communities.

The Arctic is currently experiencing some of the fastest rates of environmental change on Earth, including reductions in sea ice extent[1], melting of glaciers and ice sheets[2], lengthening of the growing season[3], thawing of permafrost[4] and intensification of the hydrologic cycle[5]. For Arctic coastal communities, perhaps the largest impact of climate warming is changes to shorefast sea ice. Shorefast ice, also known as landfast sea ice or 'fast' ice, is immobile sea ice frozen to the shore that forms along the Arctic coastline during winter and spring (Fig. 1). Shorefast ice is a stable, critically important transportation platform, connecting isolated communities and providing access to traditional hunting and fishing grounds for 3–9 months each year[6–8]. The presence of shorefast ice also mitigates coastal erosion, which threatens many Arctic communities located along subsiding coastal margins[9]. Shorefast ice is a critical habitat for marine mammals such as seals and polar bears[10], and the polynyas that form seaward of shorefast ice edges create hotspots of high ecological productivity[11]. Shorefast ice, rather than drift ice, therefore provides most of the 'sea ice services'[12] utilized by Arctic communities.

Since the early 2000s, residents of many Arctic communities have reported that shorefast ice is thinner, freezes later and breaks up earlier than in the 1990s[6,13–15]. These changes increase travel risk, reduce hunting success and threaten traditional activities[13,14,16], further exacerbating insecurity in communities already experiencing socioeconomic and cultural stress[7,15]. Despite its critical socioeconomic importance and reports of its decline, shorefast ice is challenging to observe and model and therefore has remained understudied. Shorefast ice is poorly resolved by the coarse-resolution (about 25 km) passive microwave sensors typically used to map sea ice extent, because shorefast ice forms within narrow fjords and along complex coastlines. The few studies that have analysed fine-scale changes in shorefast ice have primarily focused on Northern Alaska, notably along the coastline near Utqiagvik[17–19], whereas longer-term changes have relied on coarse-resolution models and/or observations[20,21]. Long-term changes in shorefast ice and controls on its decline therefore remain largely unknown, especially at the community scale outside of Alaska.

Here we document the timing of shorefast ice breakup from 2000 to 2018 for 28 coastal Arctic communities using daily cloud-filtered satellite imagery acquired by NASA's Moderate Resolution Imaging Spectroradiometer (MODIS). The communities are located in Nunavut and the Northwest Territories, Canada, and in Western Greenland (Fig. 2). All have strong cultural, economic, and environmental ties to shorefast ice. We compare our remotely sensed observations to surface air temperature records measured by automated weather stations (AWS) and atmospheric reanalysis (ERA-Interim) and find a strong atmospheric control on the timing of shorefast ice breakup. The strength of these correlations allows us to empirically assess the environmental sensitivity of individual communities to atmospheric warming. We then use global climate model simulations to project which communities may experience the greatest changes in shorefast ice duration by 2100. Our place-based approach allows us to determine how climate change will affect human settlements with important cultural heritage in the Arctic.

Results

Our satellite remote sensing analysis of shorefast ice breakup, defined as the first day when the 20 km radius surrounding each community reaches >90% open water (see Methods), provides a consistent 19-year breakup record for all 28 communities in Fig. 2 with an average uncertainty due to cloud cover of ±1.9 days. We find substantial variability in breakup timing across the study region, with colder communities, as defined by mean annual air temperature (MAAT), experiencing later breakup than warmer communities ($R^2 = 0.50$, $P < 0.001$). From 2000 to 2018, mean breakup timing ranged from May 29 (standard deviation ±17 days) in Uummannaq to August 1 (±10 days) in Grise Fiord, with an average date of July 11 (±15 days) across all communities. Regionally, shorefast ice cleared first in the Western Northwest Passage (June 30, ±8 days) and remained the longest in the Central Northwest Passage (July 24, ±6 days) and

[1]Department of Earth, Environmental and Planetary Sciences, Brown University, Providence, RI, USA. [2]Institute at Brown for Environment and Society, Brown University, Providence, RI, USA. [3]College of Earth, Ocean, and Atmospheric Sciences, Oregon State University, Corvallis, OR, USA. [4]Nordland Research Institute, Bodø, Norway. ✉e-mail: sarah_cooley@brown.edu

Fig. 1 | Images of shorefast sea ice. a, Seal hunter returning home by dogsled to Uummannaq, Greenland in April 2019. **b**, Shorefast ice edge roughly 15 km from Uummannaq in May 2019, 10 days before MODIS-detected breakup. **c**, Snowmobile travel on shorefast sea ice outside Iqaluit, Nunavut in March 2018. **d**, Small boat awaiting shorefast ice breakup near Iqaluit, Nunavut in March 2018 (all photos by lead author).

Northern Baffin Bay (July 23, ±7 days). On average, breakup varied by 34 days in each community over the 19-year period, ranging from a minimum of 16 days in Tuktoyaktuk to a maximum of 76 days in Ulukhaktok (Supplementary Table 1). Importantly, this interannual variability in shorefast ice breakup timing is not necessarily associated with drift ice extent, given that the correlation between shorefast breakup timing and regional drift ice extent[22] is positively significant for only 9 of 28 communities over the study period (see Supplementary Materials).

Much of the interannual variability in shorefast ice breakup is associated with local fluctuations in springtime air temperature (Fig. 3), here defined as the mean daily air temperature at 2 m above the surface during a 36-day spring period defined by the earliest date of observed shorefast ice breakup in each fjord (see Methods). Of 23 communities having at least 10 years of in situ AWS data, 18 exhibit a significant correlation between AWS springtime air temperature and breakup at 95% confidence (mean $R^2 = 0.56$) (Extended Data Fig. 1, Supplementary Table 1). Similarly, 25 of 28 communities exhibit a significant correlation at 95% confidence (mean $R^2 = 0.49$) when compared with springtime air temperature from ERA-Interim reanalysis[23] (Fig. 3; Supplementary Table 1). We hypothesize that the absence of the relationship in the other three communities is caused by persistent year-round open water near the community in Cape Dorset and a potential influence of drift ice on shorefast ice breakup detection in Ulukhaktok and Resolute. We also note that although air temperature appears to be the dominant control on breakup timing, some of the uncertainty in the correlations may be explained by winds and ocean temperatures.

While nearly all of the communities studied here exhibit strong empirical correlations between springtime air temperature and breakup, the sensitivity of the relationship (that is the slope of linear regression; Fig. 3) is highly variable between communities. Most sensitive is Grise Fiord, at −7.5 days per °C, and least sensitive is Tuktoyaktuk at −1.1 days per °C (Supplementary Table 1). Regional patterns in sensitivity are also evident, with the Northern Baffin Bay region experiencing −6.1 days per °C and Western Northwest Passage just −2.5 days per °C (Fig. 4). We find that breakup in colder communities is more sensitive to climate fluctuations than in warmer communities ($R^2 = 0.30$, $P < 0.01$; Fig. 4). This observed relationship between MAAT and sensitivity strengthens even further if the two warmest communities (Uummannaq and Sanikiluaq) are excluded ($R^2 = 0.59$, $P < 0.001$; Fig. 4a).

By applying our observed empirical correlations between springtime air temperature and shorefast ice breakup to a range of projected future air temperatures from CMIP5 global climate model simulations[24] (see Methods), we find a correspondingly wide range of projected reductions in spring shorefast ice duration. Under a high emissions scenario (IPCC Representative Concentration Pathway 8.5 (RCP8.5)), we find that by 2099, changes in breakup timing range from 5 days earlier (Tuktoyaktuk) to 44 days earlier (Taloyoak), with an average change of 20 (±9) days earlier across all communities (Supplementary Table 1). Regionally, the Central Northwest Passage is projected to experience the largest reduction in spring shorefast ice season (−31 days) and Western Northwest Passage the smallest (−12 days) (Figs. 4, 5). These overall geographical patterns are preserved under the RCP4.5 (−9 days on average) and RCP2.6 (−7 days) scenarios (Fig. 5). As with breakup sensitivity, there is a linear correlation between MAAT and predicted future change in breakup ($R^2 = 0.24$, $P = 0.01$), suggesting that colder communities will experience greater reductions in springtime shorefast ice than warmer communities (Fig. 4c). Similarly, the relationship between MAAT and predicted future change is stronger when the two warmest communities are excluded ($R^2 = 0.36$, $P < 0.01$; Fig. 4c).

Discussion

This study presents the first community-level assessment of shorefast ice breakup across northern Canada and western Greenland, thus providing insight into an understudied process that critically affects the livelihoods, cultures, and economies of coastal Arctic communities. Our analysis identifies large sub-regional variability in both the present-day timing of shorefast ice breakup and its sensitivity to future warming. Although future work is needed to

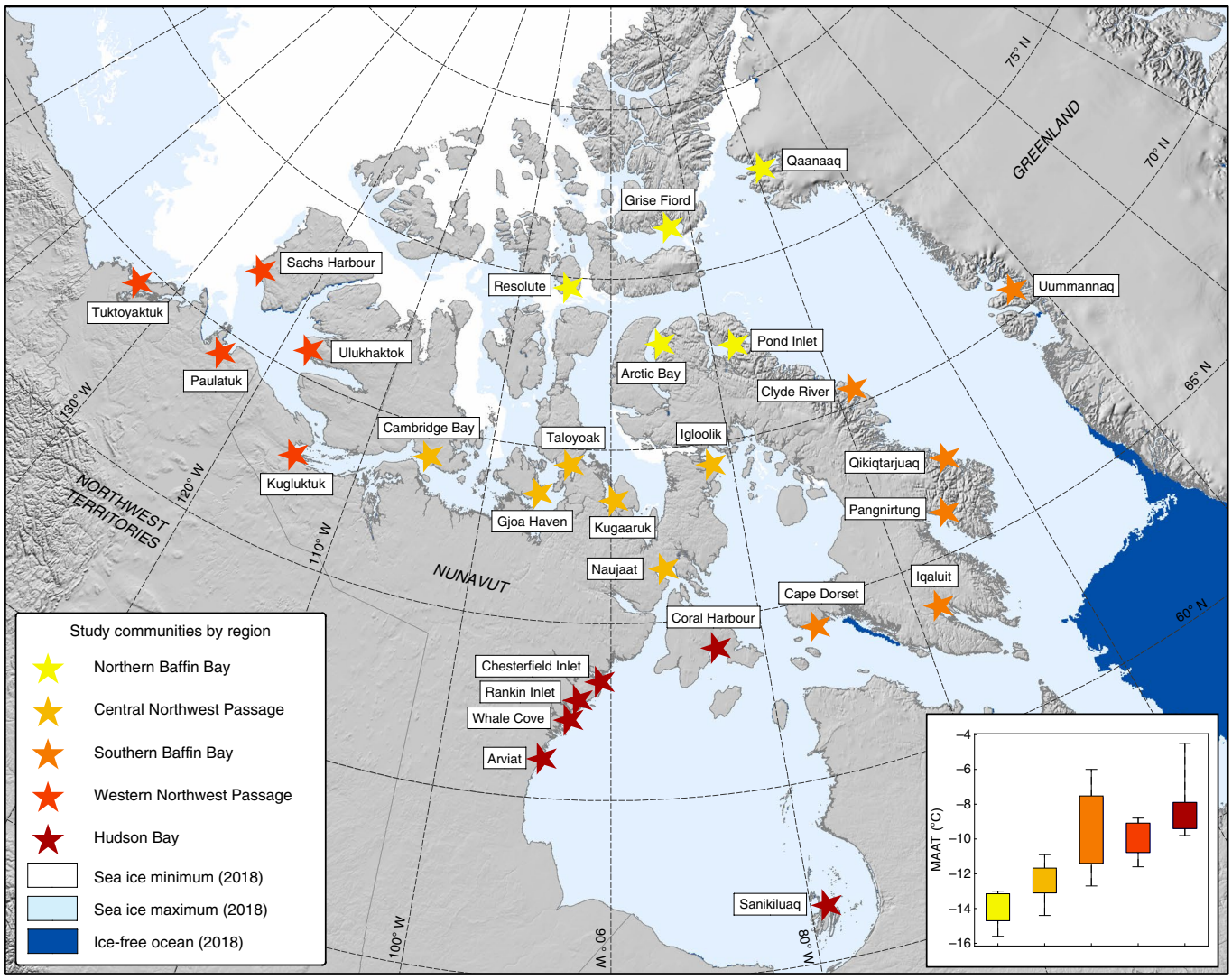

Fig. 2 | Study area map showing locations of 28 communities affected by shorefast sea ice in Nunavut and the Northwest Territories, Canada, and in western Greenland. Communities are labelled and coloured by subregion (see key). Within the ocean, white indicates the 2018 drift ice and shorefast sea ice minimum, light blue indicates the drift ice and shorefast ice maximum, and dark blue indicates perennially open ocean in 2018 as observed by NSIDC MASIE (https://nsidc.org/data/masie). Inset: box plot of MAAT over 2000–2018 for each community sub-region, where box limits represent the upper and lower quartiles and whiskers illustrate the full data range.

determine whether these findings are broadly applicable outside of the Canadian Arctic Archipelago, a clear northward trend in sensitivity is especially notable and underscores the necessity of localized approaches for assessing environmental response to Arctic climate change.

The strong positive correlations between breakup timing and springtime air temperatures over the period 2000–2018 suggest that surface–atmosphere interactions exert a first-order control on shorefast ice breakup. Few studies have specifically examined the relationship between breakup and springtime air temperature, but the strong role of atmospheric interactions helps to corroborate recent work finding surface air temperature to be the dominant control on both drift ice extent[25] and outlet glacier termini positions[26] in our study region. Although we find no statistically significant trends in air temperature or breakup timing in any community during our 19-year record, Arctic air temperatures are projected to rapidly increase over the coming decades[27]. The strongly positive correlation between springtime air temperatures and shorefast ice breakup identified here therefore suggests that breakup will occur earlier in the future, highlighting the potential exposure of coastal Arctic communities to anthropogenically induced climate warming.

While all communities are likely to experience earlier shorefast ice breakup in the future, breakup in colder communities is notably more sensitive to changes in springtime air temperature than in warmer communities (Fig. 4). This regional variability in breakup sensitivity has contrasting implications for communities in northern Canada and western Greenland, particularly when socioeconomic and cultural differences are also considered. For example, communities that are most reliant on traditional subsistence activities, such as Clyde River and Taloyoak (−6.5 and −6.9 days per °C, respectively), may be especially vulnerable to earlier ice breakup. Breakup in these two communities is expected to occur 23 to 44 days earlier, respectively, by 2099, suggesting that economically and culturally significant activities on the ice will be harder to maintain in the future[6]. Communities located along increasingly popular Arctic cruise ship routes, such as Cambridge Bay (−4.8 days per °C, −29 days in 2099) and Pond Inlet (−5.6 days per °C, −23 days in 2099), however, may experience some benefits from earlier ice

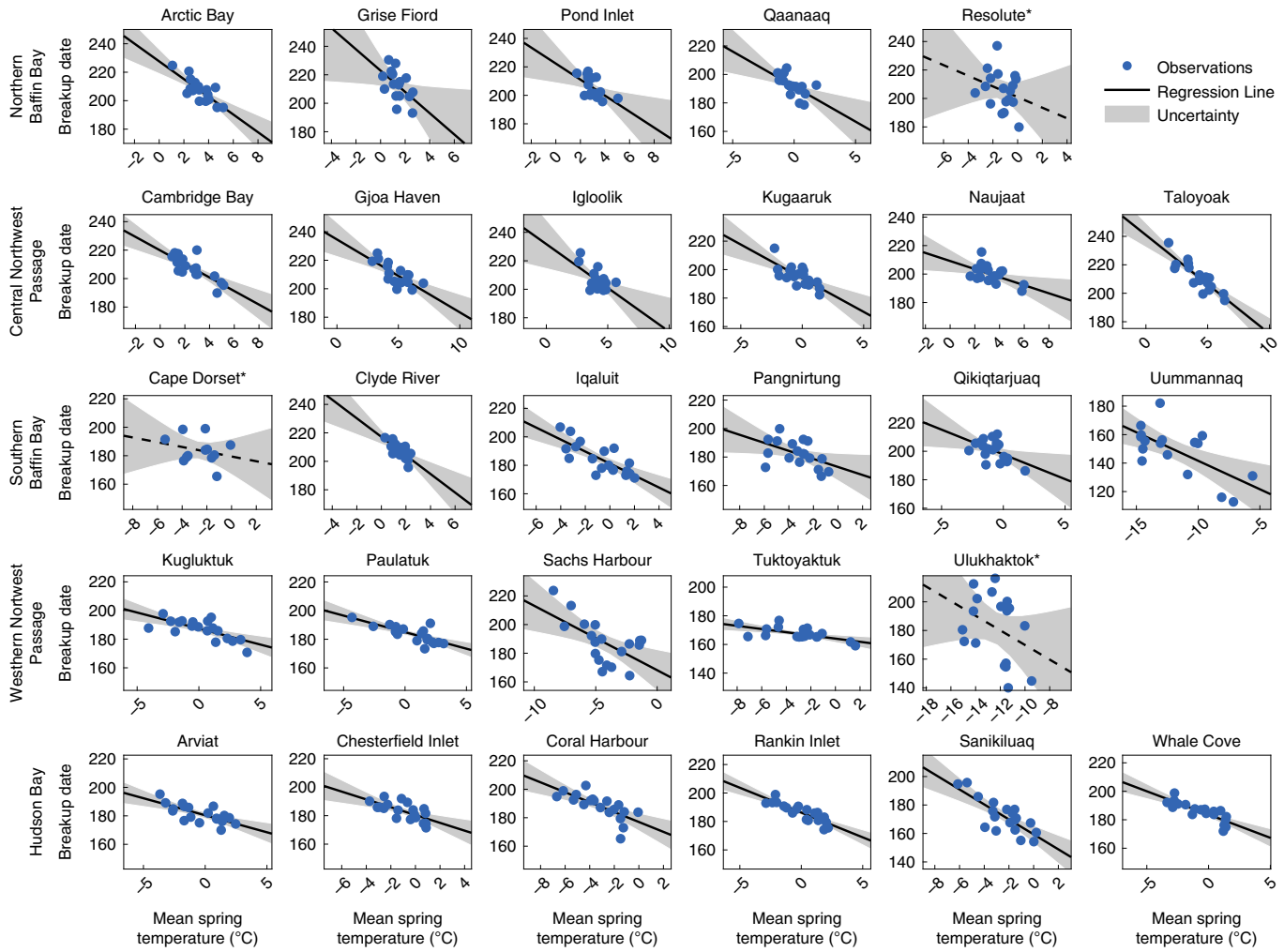

Fig. 3 | Scatter plots of shorefast ice breakup timing (day of year) versus mean springtime air temperature (°C) for all 28 communities as calculated using ERA-Interim data. Each row shows communities from the same sub-region as defined in Fig. 1. Black lines show the linear regressions between shorefast ice breakup timing and springtime air temperature, with grey shading indicating the uncertainty in this regression, calculated as the 95th confidence interval. A dashed line and a single asterisk after community name indicates communities where breakup timing and mean springtime air temperature are uncorrelated at $P < 0.05$. The *x* and *y* axes are standardized by range to illustrate the variability in slope.

breakup. Our prediction of a substantially reduced shorefast ice season in these communities has the potential to enhance economic development through increased ship visits, although rising numbers of cruise ships may also have negative environmental and cultural impacts[28].

In contrast to these examples, communities such as Tuktoyaktuk (−1.1 days per °C, −5 days in 2099) and Paulatuk (−2.3 days per °C, −11 days in 2099) may be less affected by a reduction in shorefast ice duration. Owing to its low climatic sensitivity and high potential for coastal economic development due to its new year-round connection to the North American road network[29], Tuktoyaktuk, in particular, may be less vulnerable to the cultural and economic changes caused by climate warming than other communities assessed here. These nuances emphasize the importance of taking a community-based approach to climate studies and recognizing that even within the rapidly changing Arctic, climate change does not affect all communities equally.

The results and projections presented here provide useful insight into varying spatial patterns of Arctic climate change and the exposure of coastal communities to environmental change. However, other factors beyond air temperature (such as winds, ocean temperatures and surface waves) probably also influence shorefast ice breakup timing. Similarly, breakup timing is just one of several shorefast ice metrics that affect community ice usage. Future work should thus consider incorporating additional environmental variables, together with shorefast ice thickness[30], ice stability[31] and freeze-up date[32]. Such analyses may elucidate the mechanisms controlling breakup and how they differ between warmer and colder communities, and thus provide further insight into our projections. Additional human and/or geographic factors unrelated to climate change may also influence community vulnerability to reductions in shorefast ice. For example, the two warmest communities, Uummannaq, and to a lesser extent Sanikiluaq, already experience much earlier breakup than other communities (May 29 and June 21 on average, respectively) and a shorter ice season. Therefore, the sociocultural impact of even comparatively small changes in breakup timing could be severe. This is exemplified by the 2005 winter in Uummannaq when stable shorefast sea ice never formed, meaning that locals could not access the ice and many dog teams were unused for nearly two years. In a warmer climate, such occurrences may become more frequent and lead to the loss of traditional cultural activities such as dog sledding and seal hunting on the ice[15].

Overall, our study of shorefast sea ice applies broad-scale remote sensing and climate modelling tools at a community-level to identify

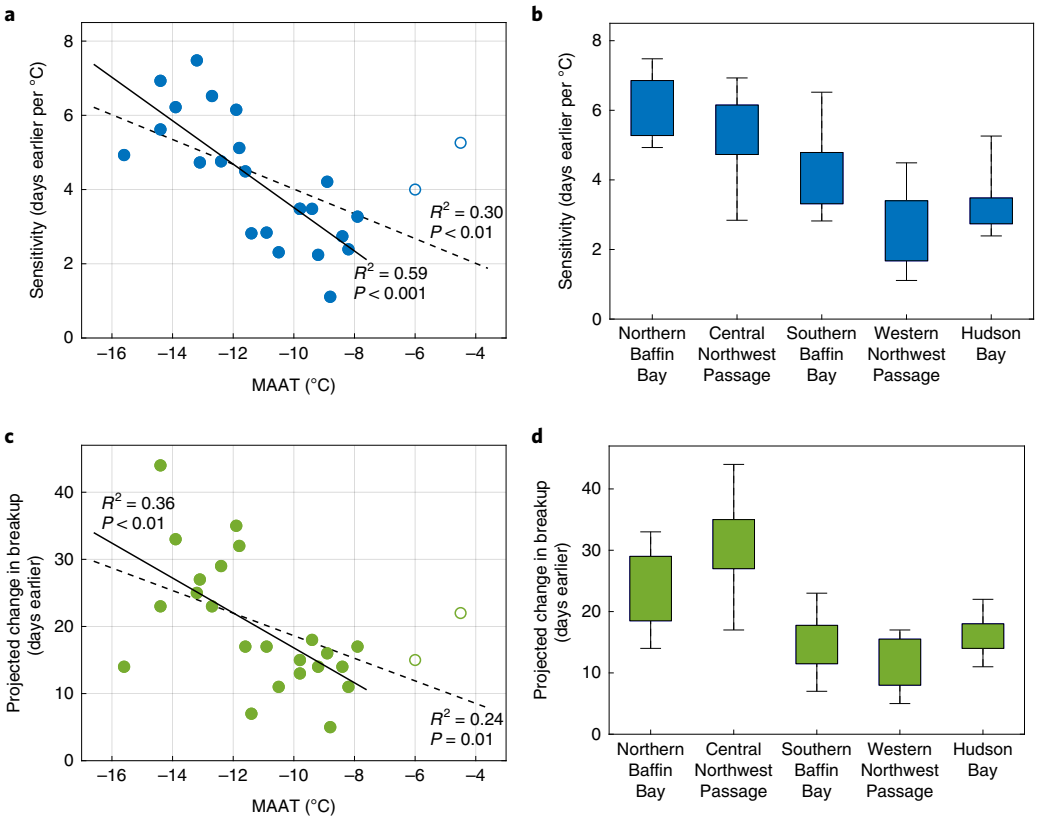

Fig. 4 | Patterns in breakup sensitivity and projected change in breakup timing by temperature and region. a, The relationship between MAAT (°C) and shorefast ice breakup sensitivity (days earlier per °C), illustrating that colder communities are more sensitive to springtime air temperature than warmer communities. **b**, Breakup sensitivity plotted by sub-region, ordered left to right from coldest to warmest. **c**, The relationship between MAAT and projected change in breakup in 2099 (days earlier), further illustrating that colder communities are likely to experience greater changes than warmer communities. **d**, Projected change in breakup in 2099 plotted by sub-region. For **a** and **c**, dashed lines show the relationship for all 28 communities, and solid lines show the relationship excluding Uummannaq and Sanikiluaq (the two warmest communities, shown as open circles on both plots). For panels **b** and **d**, box limits represent the upper and lower quartiles and the whiskers illustrate the full data range.

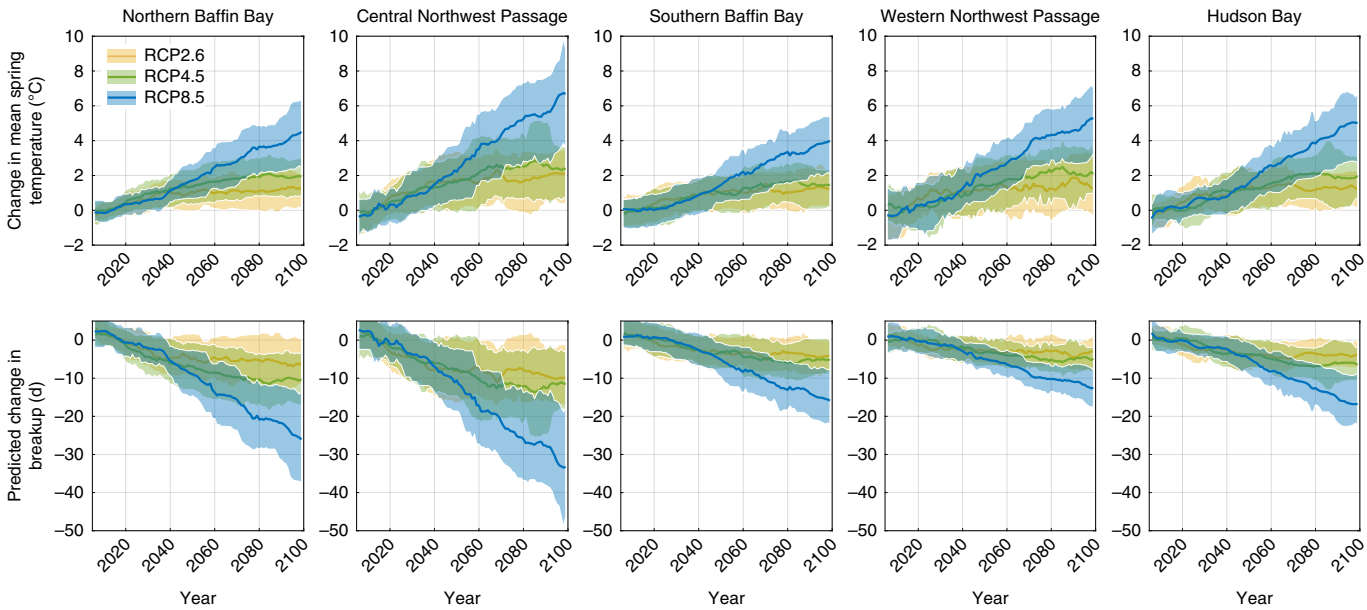

Fig. 5 | Projected changes in springtime air temperature and shorefast ice breakup using eight CMIP5 climate models. The top row shows the projected changes in springtime air temperature averaged over each sub-region for RCP2.6 (yellow), RCP4.5 (green) and RCP8.5 (blue), and the bottom row shows the corresponding projected changes in breakup timing for each sub-region. Shaded areas indicate the ensemble-averaged 25th and 75th percentile projections of all the models for each community. Sub-regions are ordered from coldest to warmest from left to right; note the much smaller projected shorefast ice reductions in Southern Baffin Bay, Western Northwest Passage and Hudson Bay compared to the colder Northern Baffin Bay and Central Northwest Passage sub-regions.

complexity at the sub-regional scale. The observed variability in shorefast sea ice appears to be localized and not necessarily correlated with pan-Arctic drift ice records, corroborating previous reports by both local residents[15] and scientists[18]. The high susceptibility of the coldest, northernmost communities of northern Canada and western Greenland to reduced shorefast ice seasons emphasizes the importance of considering the local nature of climatic changes alongside community-level differences when making policy decisions or other preparations for the consequences of climate change. Because shorefast ice is one of many environmental assets important to Arctic communities, future research combining broad-scale analysis tools with community-level characteristics may help provide more actionable information for Arctic populations facing substantial climatic and social change.

Online content

Any methods, additional references, Nature Research reporting summaries, source data, extended data, supplementary information, acknowledgements, peer review information; details of author contributions and competing interests; and statements of data and code availability are available at https://doi.org/10.1038/s41558-020-0757-5.

Received: 22 August 2019; Accepted: 17 March 2020;
Published online: 04 May 2020

References

1. Notz, D. & Stroeve, J. Observed Arctic sea-ice loss directly follows anthropogenic CO_2 emission. *Science* **354**, 747–750 (2016).
2. Mouginot, J. et al. Forty-six years of Greenland Ice Sheet mass balance from 1972 to 2018. *Proc. Natl Acad. Sci. USA* **116**, 04242 (2019).
3. Park, T., Ganguly, S., Tømmervik, H., Euskirchen, E. S. & Høgda, K. Changes in growing season duration and productivity of northern vegetation inferred from long-term remote sensing data. *Environ. Res. Lett.* **11**, 084001 (2016).
4. Biskaborn, B. K. et al. Permafrost is warming at a global scale. *Nat. Commun.* **10**, 264 (2019).
5. Rawlins, M. A. et al. Analysis of the Arctic system for freshwater cycle intensification: observations and expectations. *J. Clim.* **23**, 5715–5737 (2010).
6. Gearheard, S. et al. 'It's Not that Simple': a collaborative comparison of sea ice environments, their uses, observed changes, and adaptations in Barrow, Alaska, USA, and Clyde River, Nunavut, Canada. *Ambio* **35**, 203–211 (2006).
7. Ford, J. D. et al. Sea ice, climate change, and community vulnerability in northern Foxe Basin, Canada. *Clim. Res.* **38**, 137–154 (2009).
8. Mahoney, A. R. in *Arctic Report Card 2018* (eds Osborne, E., Richter-Menge, J. A. & Jeffries, M. O.) 99–109 (National Oceanic and Atmospheric Administration, 2018).
9. Overeem, I. et al. Sea ice loss enhances wave action at the Arctic coast. *Geophys. Res. Lett.* **38**, L17503 (2011).
10. Laidre, K. L. et al. Quantifying the sensitivity of Arctic marine mammals to climate-induced habitat change. *Ecol. Appl.* **18**, 97–125 (2008).
11. Mundy, C. J. et al. Contribution of under-ice primary production to an ice-edge upwelling phytoplankton bloom in the Canadian Beaufort Sea. *Geophys. Res. Lett.* **36**, L17601 (2009).
12. Eicken, H., Lovecraft, A. L. & Druckenmiller, M. L. Sea-Ice System Services: a framework to help identify and meet information needs relevant for Arctic observing networks. *Arctic* **62**, 119–136 (2009).
13. Laidler, G. J. et al. Travelling and hunting in a changing Arctic: assessing Inuit vulnerability to sea ice change in Igloolik, Nunavut. *Clim. Change* **94**, 363–397 (2009).
14. Meier, W. N., Stroeve, J. & Gearheard, S. Bridging perspectives from remote sensing and Inuit communities on changing sea-ice cover in the Baffin Bay region. *Ann. Glaciol.* **44**, 433–438 (2006).
15. Baztan, J., Cordier, M., Huctin, J. & Zhu, Z. Life on thin ice: insights from Uummannaq, Greenland for connecting climate science with Arctic communities. *Polar Sci.* **13**, 100–108 (2017).
16. Pearce, T., Smit, B. & Ford, J. D. Inuit vulnerability and adaptive capacity to climate change in Ulukhaktok, Northwest Territories, Canada. *Polar Rec.* **46**, 157–177 (2010).
17. Mahoney, A., Eicken, H., Gaylord, A. G. & Shapiro, L. Alaska landfast sea ice: Links with bathymetry and atmospheric circulation. *J. Geophys. Res.* **112**, C02001 (2007).
18. Mahoney, A. R., Eicken, H., Gaylord, A. G. & Gens, R. Landfast sea ice extent in the Chukchi and Beaufort Seas: the annual cycle and decadal variability. *Cold Reg. Sci. Technol.* **103**, 41–56 (2014).
19. Petrich, C. et al. Coastal landfast sea ice decay and breakup in northern Alaska: key processes and seasonal prediction. *J. Geophys. Res.* **117**, C02003 (2012).
20. Howell, S. E. L., Laliberté, F., Kwok, R., Derksen, C. & King, J. Landfast ice thickness in the Canadian Arctic Archipelago from observations and models. *Cryosphere* **10**, 1463–1475 (2016).
21. Galley, R. J., Else, B. G. T., Howell, S. E. L., Lukovich, J. V. & Barber, D. G. Landfast sea ice conditions in the Canadian Arctic: 1983-2009. *Arctic* **65**, 133–144 (2012).
22. Fetterer, F., Knowles, K., Meier, W. H., Savoie, M. & Windnagel, A. K. *Sea Ice Index* Version 3 (National Snow and Ice Data Center, 2017); https://doi.org/10.7265/N5K072F8
23. Dee, D. P. et al. The ERA-Interim reanalysis: configuration and performance of the data assimilation system. *Q. J. R. Meteorol. Soc.* **137**, 553–597 (2011).
24. Taylor, K. E., Stouffer, R. J. & Meehl, G. A. An overview of CMIP5 and the experiment design. *Bull. Am. Meteorol. Soc.* **93**, 485–498 (2012).
25. Olonscheck, D., Mauritsen, T. & Notz, D. Arctic sea-ice variability is primarily driven by atmospheric temperature fluctuations. *Nat. Geosci.* **12**, 430–434 (2019).
26. Cook, A. J. et al. Atmospheric forcing of rapid marine-terminating glacier retreat in the Canadian Arctic Archipelago. *Sci. Adv.* **5**, eaau8507 (2019).
27. Pithan, F. & Mauritsen, T. Arctic amplification dominated by temperature feedbacks in contemporary climate models. *Nat. Geosci.* **7**, 181–184 (2014).
28. Stewart, E. J., Howell, S. E. L., Draper, D., Yackel, J. & Tivy, A. Sea ice in Canada's arctic: implications for cruise tourism. *Arctic* **60**, 370–380 (2007).
29. Bennett, M. M. From state-initiated to Indigenous-driven infrastructure: the Inuvialuit and Canada's first highway to the Arctic Ocean. *World Dev.* **109**, 134–148 (2018).
30. Dumas, J. A., Flato, G. M. & Brown, R. D. Future projections of landfast ice thickness and duration in the Canadian Arctic. *J. Clim.* **19**, 5175–5189 (2006).
31. Dammann, D. O., Eriksson, L. E. B., Mahoney, A. R., Eicken, H. & Meyer, F. J. Mapping pan-Arctic landfast sea ice stability using Sentinel-1 interferometry. *Cryosphere* **13**, 557–577 (2019).
32. Yu, Y., Stern, H., Fowler, C., Fetterer, F. & Maslanik, J. Interannual variability of Arctic landfast ice between 1976 and 2007. *J. Clim.* **27**, 227–243 (2014).

Methods

Satellite imagery. Shorefast ice was mapped using the atmospherically corrected MODIS Level 2 product, MOD09GQ, a daily product with a ground sampling resolution of 250 m (Supplementary Fig. 1) produced from the Moderate Resolution Imaging Spectroradiometer aboard NASA's Terra satellite[33]. The high temporal and spatial resolution of MOD09GQ allowed us to distinguish shorefast ice in narrow Arctic fjords with sufficiently fine resolution to resolve the timing of breakup accurately. Clouds and cloud shadows were masked using the cloud mask from coincident MOD09GA products which were resampled (nearest neighbours) from 1,000 m to 250 m pixel resolution to match the MOD09GQ products. We analysed all daily imagery collected between day of year 60 and 240 (March 1 to August 28) over 2000–2018.

Breakup detection. Our classification and breakup detection method builds on the river ice breakup detection method presented in Cooley and Pavelsky (2016)[34]. First, we created a land/ocean mask using high-resolution coastline shapefiles from Statistics Canada (https://open.canada.ca/data/en/dataset/a883eb14-0c0e-45c4-b8c4-b54c4a819edb) and GADM (https://gadm.org/index.html), which were combined with the resampled MOD09GA cloud masks to exclude all land and cloudy pixels in the MOD09GQ images. Each MODIS band 2 (841–876 nm) image was then classified into snow, ice and water using simple thresholds in band 2 reflectance (<0.1 for water, 0.1–0.5 for ice and >0.5 for snow; reflectance is the MOD09GQ digital number multiplied by 0.001). Next, we applied a 5 km × 5 km grid covering the fjord and/or coastal ocean within about 20 km of each community to each image and determined the percentage of cloud-free MODIS pixels that were classified as snow, water and ice for each grid cell. This produced a daily time series of snow, ice and water percentage for each grid cell from March to August for every year between 2000 and 2018 (Extended Data Fig. 2).

Using these time series, we determined the annual date of breakup for each 5 km × 5 km grid cell. First, all days with >50% cloud cover were removed and Hampel and 5-day median filters were applied to the time series to remove outliers caused by sensor noise or failure of the MODIS cloud mask. Only grid cells which had a snow or ice value >90% for at least three consecutive cloud-free observations in each year were analysed to ensure that shorefast ice was present. Breakup date detection proceeded for each time series as follows:

(1) We identified the first five-observation period when the grid cell averaged at least 50% open water.
(2) We determined the first day within or following this five-observation period when the grid cell reached 90% open water.
(3) To account for cloud cover, the breakup date was then defined as the midpoint between this date and the previous cloud-free observation, with the uncertainty in breakup detection the difference between the two[34] (Extended Data Fig. 2).

This process was repeated for all grid cells within 20 km of the community for all years, which yielded a mean uncertainty in breakup timing due to cloud obscuration of ±1.9 days. We defined the breakup date for each individual community for each year as the mean breakup timing in these grid cells. Breakup dates were allowed to be fractional during the temperature analysis, but for simplicity were rounded to the nearest day in the table and in the text. While we acknowledge that community use of shorefast ice generally ceases before the fjord is 90% open water, we chose this breakup threshold because it is a consistent metric that is interpretable to both scientists and local community members as the point in which the area surrounding each community becomes clear of ice. To mitigate the possible influence of drift ice on breakup detection, grid cells that on average do not transition from >90% ice to >90% water each spring/summer were removed from the analysis, because in our manual examination of the imagery, grid cells in our study area containing substantial drift ice tended to have this characteristic. We note that this method does not explicitly distinguish between drift ice and shorefast ice. While this distinction is not required along the complex coastlines and fjords of the Canadian Arctic Archipelago and western Greenland where nearly all sea ice is landlocked, we caution against the use of this approach in regions of the Arctic where shorefast ice is less extensive, such as along the Bering and Chukchi coasts in Alaska.

We assessed the accuracy of this method first through sensitivity analysis of the water thresholds. Water reflectance thresholds of 0.08, 0.09, 0.10 (chosen threshold), 0.11 and 0.12 were tested for three communities over the full MODIS record. Changes to the threshold had comparatively small impacts on breakup timing, shifting breakup by only 0–4 days on average (Supplementary Fig. 2), and had little to no impact on correlations with air temperature. Therefore, although the choice of water threshold may slightly shift the exact date of breakup, it is unlikely to affect any of our conclusions.

We also assessed the accuracy of this method using high-resolution Planet Labs and Sentinel-2 imagery (both available from https://www.planet.com/explorer/)[35]. We compared the breakup dates for each community in 2017 and 2018 with breakup dates manually detected using high resolution, near-daily Planet Labs and Sentinel-2 satellite imagery. This comparison was imperfect because there are biases associated with manual detection and furthermore cloud cover and missing imagery can affect results when comparing between sensors. However, it was a useful external check on the automatically derived breakup dates to ensure accuracy of the method. For both 2017 and 2018, manually and automatically detected breakup dates were strongly correlated, with an $R^2 > 0.93$. The root-mean-square error between manually and automatically detected dates was 4.3 days in 2017 and 4.2 days for 2018, and the median difference between the dates was 1.8 days for 2017 and 3.4 days for 2018, suggesting confidence in our breakup detection method (Supplementary Fig. 3).

Temperature analyses. To assess the relationship between breakup timing and springtime air temperature we used both AWS data from each community and the ERA-Interim reanalysis product[23]. For Canadian communities, hourly AWS data were obtained from the Government of Canada Historical Weather Data (http://climate.weather.gc.ca/). For Greenlandic communities, hourly AWS data were obtained from Danish Meteorological Institute (https://www.dmi.dk/publikationer/). All hourly data were averaged to a daily mean, and to avoid bias caused by diurnal temperature variability, days with less than 22 hours of data were excluded. To produce the yearly springtime air temperature records, we averaged between stations if multiple stations were available and interpolated between days if data was missing. Years where more than 4 days of spring air temperature were missing were excluded to limit the effect this bias could have on reported results. Overall, 23 of 28 communities had AWS data meeting these standards for >10 years over the period 2000–2018.

We also used ERA-Interim reanalysis data[23] because it provides a consistent record available over all 28 communities between 2000–2018 (https://www.ecmwf.int/en/forecasts/datasets/reanalysis-datasets/era-interim) and has been shown to perform well over the Arctic[36]. To produce the springtime air temperature time series, six-hourly temperature values from the nearest four ERA-Interim grid cells to each community were averaged into a daily time series.

For both AWS and ERA-Interim datasets, we calculated the mean air temperatures (in °C) for each community over a set period in the spring:

$$T_s = \sum_{\mathrm{EoS}-40}^{\mathrm{EoS}-5} T_d \,/36 \quad (1)$$

where T_s is the mean springtime air temperature (in °C), EoS is the end of spring and T_d is the daily air temperature (in °C). We defined the 'end of spring' as the earliest date of breakup for each community, which ranged from 22 April to 17 July. This ensured that our calculation of springtime air temperature encompassed the period prior to breakup for each community given the wide range in breakup timing. To determine the length of the period prior to the 'end of spring' which best predicts breakup timing, we optimized for maximum average R^2 over all communities and tested between 15 and 75 days prior to the earliest breakup. We excluded the five days prior to the end of spring to ensure that the mean springtime temperature was calculated only over days with near-complete ice cover, thus mitigating any potential effect of a positive feedback between open water and air temperature[17]. This analysis yielded 40 days prior to the end of spring as the optimal period over which to calculate mean springtime air temperature, though changing the number of days prior to the end of breakup from 35 to 45 days has little impact on correlations with air temperature.

To estimate future changes in breakup, we used daily 2 m air temperature outputs from eight CMIP5 global climate models, namely BNU-ESM, CCSM4, CESM1-CAM5, CSIRO-Mk3-6-0, GFDL-CM3, IPSL-CM5A-LR, NorESM1 and BCC-CSM1[24]. These eight model runs were chosen as they all provide daily 2 m air temperature data over 2006–2099 under RCP2.6 (low emission), RCP4.5 (midrange mitigation) and RCP8.5 (high emissions) scenarios. The yearly springtime air temperature time series were produced by averaging the daily temperature time series for all grid cells located within a 2° × 2° box surrounding each community and calculating mean springtime air temperature as described above. We chose this sampling strategy due to inconsistencies in CMIP5 model resolutions. Next, all 94-year modelled springtime air temperature time series were normalized to their 2006–2018 average, and a 10-year median filter was applied. We then calculated projected future changes in breakup timing by applying the air temperature sensitivities, calculated using ERA-Interim and normalized to 2006–2018, to the future springtime air temperature time series.

Data availability

All data needed to evaluate the conclusions of this paper are present in the paper and/or the Supplementary Information. Additional data related to the paper may be requested from the authors. All data can also be accessed online from the following data centres: MOD09GQ and MOD09GA data from https://lpdaac.usgs.gov, maintained by the NASA EOSDIS LP DAAC at the USGS/EROS Center, Sioux Falls, South Dakota; AWS data from http://climate.weather.gc.ca/ (Canada) and https://www.dmi.dk/publikationer/ (Greenland); ERA-Interim data from the European Centre for Medium-Range Weather Forecast at https://www.ecmwf.int/en/forecasts/datasets/reanalysis-datasets/era-interim; and CMIP5 climate model outputs from https://esgf-node.llnl.gov/projects/cmip5/.

Code availability

The codes used in this study are available at: https://github.com/sarahwcooley/shorefast-sea-ice-breakup[37].

References

33. Vermote, E. F. & Wolfe, R. *MOD09GQ MODIS/Terra Surface Reflectance Daily L2G Global 250m SIN Grid V006* (NASA EOSDIS Land Processes DAAC, 2015); https://doi.org/10.5067/MODIS/MOD09GQ.006
34. Cooley, S. W. & Pavelsky, T. M. Spatial and temporal patterns in Arctic river ice breakup revealed by automated ice detection from MODIS imagery. *Remote Sens. Environ.* **175**, 310–322 (2016).
35. *Planet Application Program Interface: In Space for Life on Earth* (Planet Team, 2019); https://api.planet.com
36. Lindsay, R., Wensnahan, M., Schweiger, A. & Zhang, J. Evaluation of seven different atmospheric reanalysis products in the Arctic. *J. Clim.* **27**, 2588–2606 (2014).
37. Cooley, S. W. *Shorefast Sea Ice Breakup Detection Workflow* First release (2020); https://doi.org/10.5281/zenodo.3699663

Acknowledgements

This research was funded by an NSF Navigating the New Arctic (NNA) grant (no. 1836473) managed by R. Delgado. S.W.C. acknowledges funding from an NSF Graduate Research Fellowship and from a Geological Society of America Student Research Grant. J.C.R. acknowledges funding from a Voss Postdoctoral Fellowship. We gratefully acknowledge A. Andreasen, the Uummannaq Polar Institute and the Uummannaq Children's Home for providing lodging and fieldwork support. We thank P. Kreutzmann and M. Johansen for sharing knowledge and for their assistance in the field. We acknowledge the World Climate Research Programme's Working Group on Coupled Modeling, which is responsible for CMIP, and we thank the climate modelling groups listed in the Methods for producing and making available their model output.

Author contributions

S.W.C. and J.C.R. conceived the project. S.W.C. developed the methodology, carried out the data analysis and wrote the manuscript. J.C.R. acquired the funding and co-wrote the manuscript. L.C.S. provided supervision and co-wrote the manuscript. B.P. and C.H. assisted with the development of the methodology and edited the manuscript. B.D. and A.H.L. edited the manuscript.

Competing interests

The authors declare no competing interests.

Additional information

Extended data is available for this paper at https://doi.org/10.1038/s41558-020-0757-5.

Supplementary information is available for this paper at https://doi.org/10.1038/s41558-020-0757-5.

Correspondence and requests for materials should be addressed to S.W.C.

Peer review information *Nature Climate Change* thanks Walter Meier and the other, anonymous, reviewer(s) for their contribution to the peer review of this work.

Reprints and permissions information is available at www.nature.com/reprints.

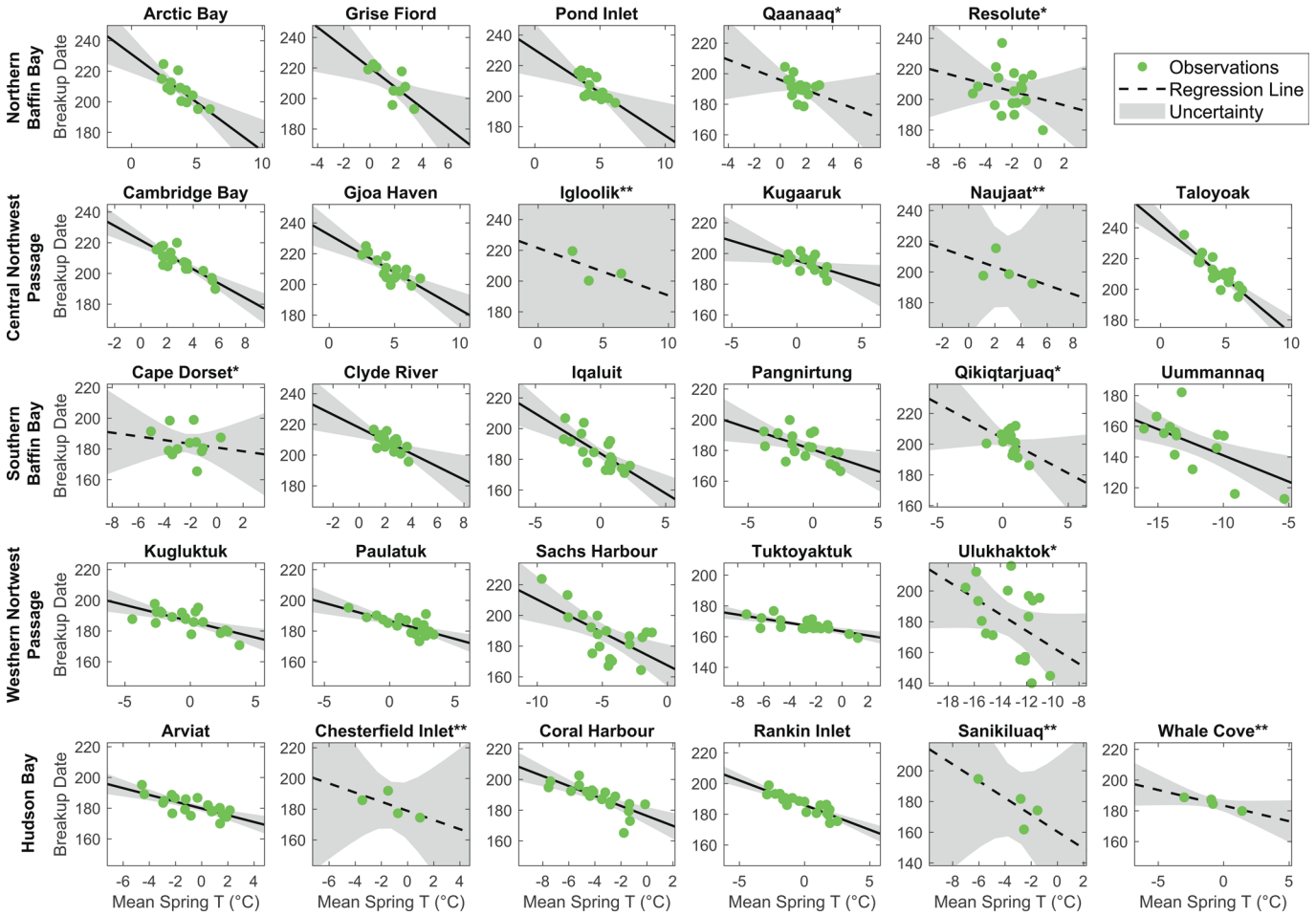

Extended Data Fig. 1 | Scatter plots of shorefast ice breakup timing (day of year) versus mean springtime air temperature (°C) for all 28 communities as calculated using AWS data. Each row shows communities from the same sub-region as defined in Fig. 1. Black lines show the linear regressions between shorefast ice breakup timing and springtime air temperature, with grey shading indicating the uncertainty in this regression. Single asterisk after community name indicates communities where breakup timing and mean springtime air temperature are uncorrelated at $p < 0.05$; double asterisk after community name indicates communities with less than 10 years of AWS data. The *x* and *y* axes are standardized by range to illustrate the variability in slope.

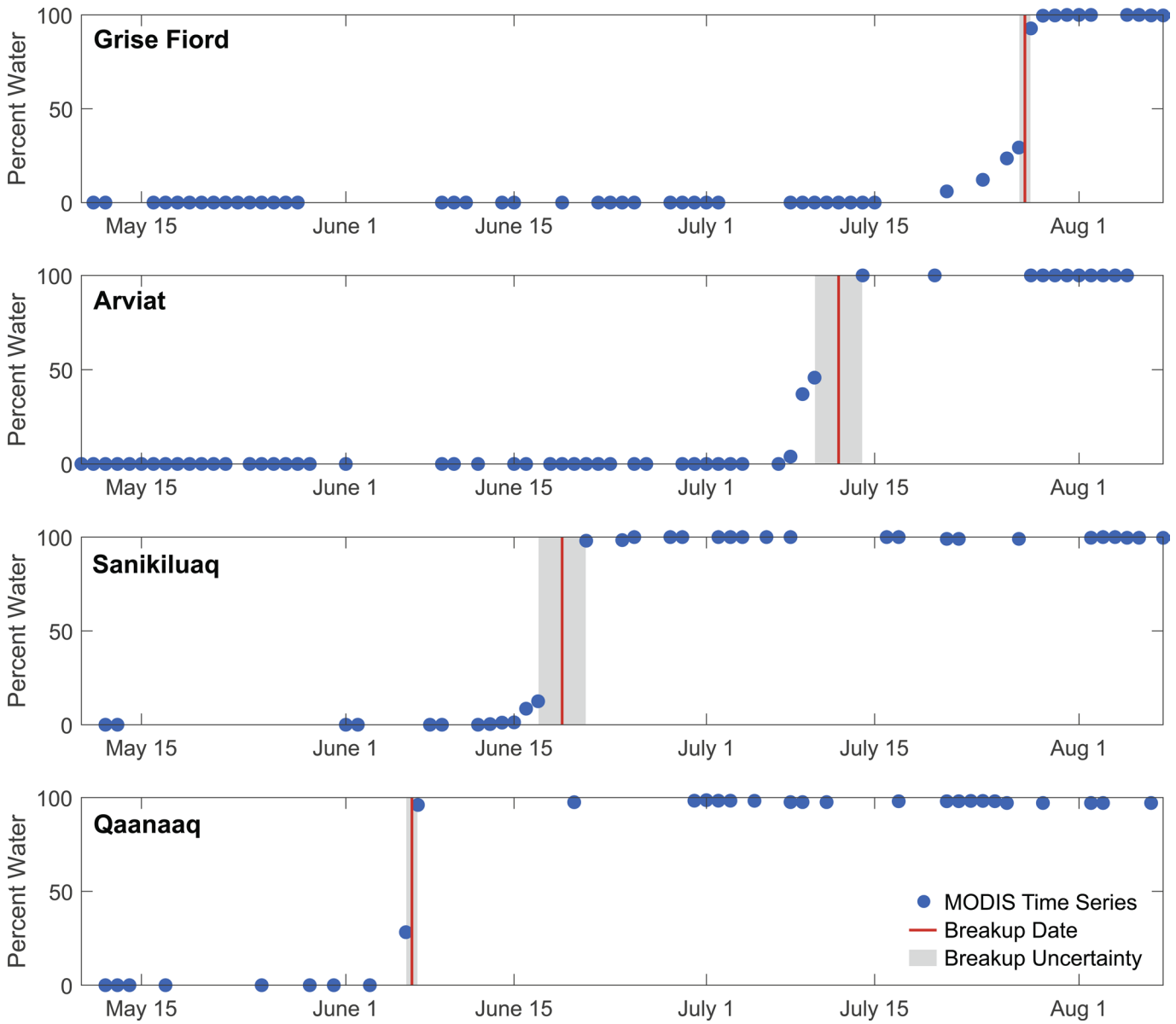

Extended Data Fig. 2 | Example of MODIS-derived percentage water time series for grid cells located near four communities in 2006. The blue circles represent the MODIS time series after cloud removal and median filtering. The red line represents the detected breakup date, defined as the mid-point of the first day when the grid cell contains greater than 90% water and the previous observation. The grey-shaded region represents the uncertainty due to cloud cover.